Bombardment-Induced Tunable Superlattices in the Growth of Au-Ni Films

J. H. He,* C. A. Carosella, G. K. Hubler, S. B. Qadri, and J. A. Sprague
Naval Research Laboratory, Washington, DC 20375, USA
(Received 23 September 2005; published 10 February 2006)

Highly ordered superlattices are typically created through the sequential deposition of two different materials. Here, we report our experimental observation of spontaneous formation of superlattices in coevaporation of Au and Ni under energetic ion bombardment. The superlattice periodicities are on the order of a few nanometers and can be adjusted through the energy and flux of ion beams. Such a self-organization process is a consequence of the bombardment-induced segregation and uphill diffusion within the advancing nanoscale subsurface zone in the film growth. Our observations suggest that ion beams can be employed to make tunable natural superlattices in the deposition of phase-separated systems with strong bombardment-induced segregation.

DOI: 10.1103/PhysRevLett.96.056105 PACS numbers: 81.07.−b, 61.10.Kw, 61.80.Jh

Fabrication of nanosized patterns has attracted much attention in recent years due to its potential applications in development of functional materials and nanodevices. Of particular interest is to create the periodically structured materials at the nanometer scale through spontaneous processes during the thin film deposition. These self-organized nanostructures include strain-driven quantum dots [1], anisotropy-induced nanowires [2], and superlattices [3–6]. The spontaneous formation of superlattice structures has been observed in the III-V and II-VI alloys during molecular beam epitaxy (MBE) [3–5], probably due to phase separation. There have also been reports on the formation of $Si_{1-x}Ge_x$ superlattices in MBE through the growth on highly vicinal surfaces, due to the biased incorporation of atoms at different steps in a modulated local strain field [6]. Recently, Foo *et al.* attributed their observation of a $Si_{1-y}C_y$ superlattice in a gas-source MBE to a self-arresting feedback loop in the surface-reaction pathways [7]. Additionally, multilayers can be formed in co-disposition of low-energy mass selected carbon and metal ions [8].

In this Letter, we for the first time show our experimental observation of tunable superlattice formation in ion beam assisted deposition (IBAD) of gold and nickel. The Au-Ni phase diagram [9] indicates that Au and Ni have a very limited mutual solubility; supersaturated solid solutions can thus be formed in almost the whole composition range. They decompose into two phases through spinodal decomposition. Such a phase separation generally produces domain structures in a random way, even on a nanoscale level [10]. The transition from a random structure to periodic one suggests that a physical force alters the phase separation process. We are aware of the formation of quasiperiodic patterns in the wake of a moving reaction front, a phenomenon commonly called *Liesegang rings* [11], and the observation of surface-directed spinodal decomposition wave due to the preferential wetting of an existing static surface [12]. Ion bombardment of a growing film produces both bombardment-induced segregation normal to the film surface [13,14] and an advancing nanoscale subsurface diffusion zone, within which spinodal decomposition (uphill diffusion) is effective. As such, the interplay of segregation and phase separation can produce a positive feedback loop guided by ion beams to form compositional modulations along the growth direction.

We choose a binary metallic system of Au-Ni for this study because both phase separation and bombardment-induced segregation [14] are well understood in this alloy. Au-Ni thin films were prepared by coevaporating gold and nickel on Si (100) substrates at nominal room temperature in a vacuum system with a base pressure of 5×10^{-9} Torr. The deposition rates were kept constant at all times by feedback control of *e*-beam current after stabilization of evaporation sources. The nominal values were approximately 0.3 Å/s for Au and 0.9 Å/s for nickel. The film thickness is between 1500 Å and 3000 Å. During the deposition, the growing film was bombarded with Ar^+ ions at energy of 100–800 eV and beam current of 25 or 50 $\mu A/cm^2$. A few tens of degrees (30–60 °C, dependent on ion energy and flux) increase was observed at a physically separated location near the rotated substrate during film growth, using a thermal couple. Local temperature rise would be even higher in the thin film that the ions penetrate. The corresponding thin film without ion bombardment was also prepared for comparison. We applied x-ray reflectivity (XRR) to characterize the composition along the growth direction. XRR can detect the electron density profile normal to the surface of thin film with a depth resolution of a few angstroms. It is a suitable technique to study Au-Ni thin films since the electron densities of Au and Ni are significantly different. XRR data were collected using summations to improve signal to background ratio in a Riguka two-circle diffractometer with Cu K_α radiation. The off-specular background was measured at offset of 0.10° and subtracted from the specular measurement to obtain the true specular spectrum.

Figure 1 presents a true specular XRR of the Au-Ni film deposited on Si (100) at room temperature under Ar^+

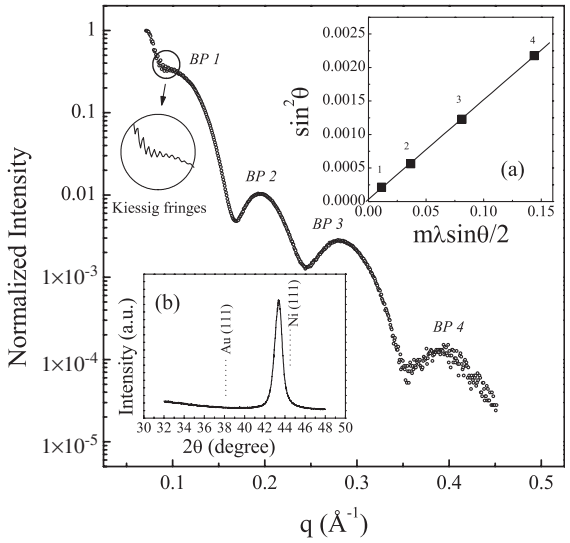

FIG. 1. True specular x-ray reflectivity (θ–2θ scan) shows both Kiessig peaks (enlarged part) and Bragg peaks (identified as $BP1$, $BP2$, etc.) due to existence of superlattice structure. The inset (a) shows fitting of Bragg peak positions using modified Bragg law and (b) is the x-ray diffraction pattern for 2θ between 32° and 48°, indicating Au-Ni solid solutions are formed.

bombardment at 800 eV and 25 μA/cm^2 ($\sim 1.6 \times 10^{14}$ Ar$^+$/cm^2 s). The Bragg peaks in XRR unambiguously indicate the formation of superlattice structures. As shown in the inset (a), the multilayer periodicity d is calculated as 6.7 nm using the modified Bragg equation $2d\sin\theta(1 - \delta/\sin^2\theta) = m\lambda$ [15] by fitting $\sin^2\theta$ versus $m\lambda\sin\theta/2$ for identified Bragg peak positions, where δ is the average deviation of the refractive index from unity. Assuming a linear combination of δ's for Au and Ni, the fitted δ gives an average composition of Au around 12.7%, which is less than its nominal value (17.7%). The reduced Au composition suggests that ion beams preferentially sputter Au atoms in Au-Ni alloys [16]. Furthermore, we quantitatively obtain the electron density profile by fitting to the XRR data scaled by the Frensnel reflectivity R_F in the kinematical approximation,

$$\frac{R(q_z)}{R_F(q_z)} = \left| \frac{1}{\rho_0} \int \frac{\partial \rho}{\partial z} e^{-iq'z} dz \right|^2 \qquad q' = (q^2 - q_c^2)^{1/2},$$

where ρ is the average electron density, q_c is the critical wave vector for total external reflection, and ρ_0 is the bulk electron density. We employed a hybrid of genetic algorithm and simulated annealing for optimization [17]. The electron densities of slabs were varied both individually and in sine oscillations of wavelength on a scale of 2–10 nm. The best fit of reflectivity gives the electron density profile in the direction normal to the surface. The Au-Ni film has an average electron density around 2.9 e^-/Å^3. The electron density oscillations show an amplitude variation of ± 0.12 e^-/Å^3 and a wavelength around 6.7 nm. Assuming linear combination of electron densities of Au and Ni, the Au-Ni film has an average Au composition of 16 at. % with variations around ± 8 at. %. The observed compositional modulation is not a local property of the deposited film, since XRR has a large sampling area. In addition, no large precipitates were found from the x-ray diffraction (XRD) pattern as shown in the inset (b) of Fig. 1. The Ni-rich supersaturated fcc solid solutions with an average lattice parameter of 3.61 Å are formed in the Au-Ni film since we only observed a single shifted broad peak around Ni(111) and Au(111) positions in the XRD pattern. The average grain size is around 10 nm based on the Scherrer's formula without considering the strain-induced peak broadening.

Furthermore, we show through XRR measurements in Fig. 2 that the superlattice structures are dependent upon the ion energy and flux. The variation of Bragg peak spans and intensities for different deposition conditions in Fig. 2(a) evidences that ion beams produce compositional modulations with different periodicities and amplitudes in the Au-Ni films. There are no clear Bragg peaks for the Au-Ni film deposited without ion bombardment, suggesting that the compositional modulation does not exist. We used

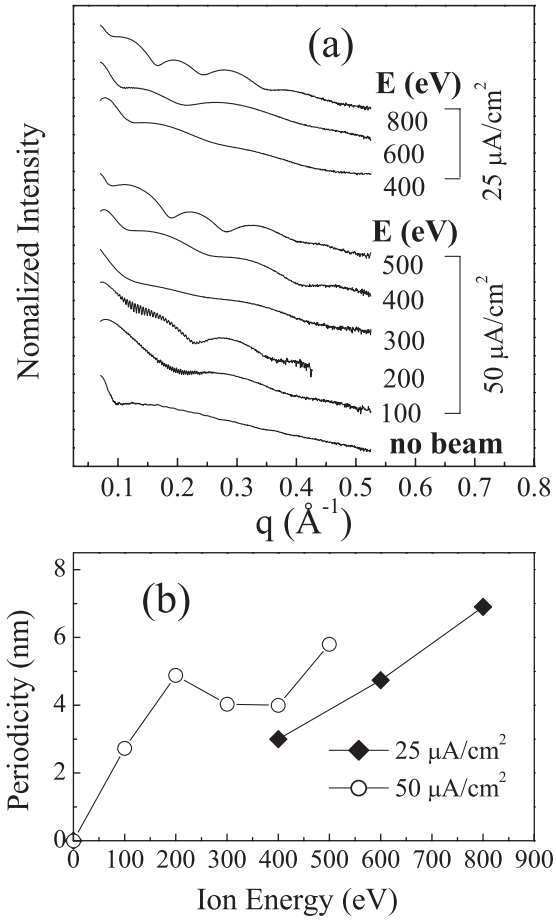

FIG. 2. Dependence of superlattice structures upon the bombarded ion energy and flux. (a) Specular x-ray reflectivity measurements, showing variations of intensities and positions of Bragg peaks. (b) Superlattice periodicity vs ion energy and flux.

the modified Bragg law or simple Bragg law to estimate the superlattice periodicities and plotted them in Fig. 2(b). At ion energies greater than 400 eV, the compositional modulation of Au-Ni films has a large amplitude and periodicity with increasing ion energy. At low ion energies, the superlattice periodicity does not monotonically increase with ion energy. There is obviously a kink around 300–400 eV, as shown in the data for beam current of 50 μA/cm^2. Such a complex behavior may be associated with synergistic effects of several processes in the ion bombardment.

The observed tunable superlattice structures in the Au-Ni films must arise from the redistribution of species during IBAD as they are correlated to ion energy and flux. Step-flow growth may play a role if the diffusion is restricted to the surface [6]. Also, if the surface diffusion is negligible relative to bulk diffusion, compositional wave itself may drive the formation of superlattices [18]. However, under ion bombardment both surface and subsurface diffusion processes are important. Ion beams not only induce a local temperature rise but also produce a large number of radiation-induced defects. We thus provide an alternative model based on mass transport within the nanoscale subsurface zone formed by penetrating energetic ions. We consider two competing driving forces for mass transport within the nanoscale subsurface zone. The first one results from the chemical interactions. In a supersaturated Au-Ni solid solution, one expects strong radiation-enhanced spinodal decomposition (uphill diffusion), giving the mass flow of $J_A^{\rm chem}$ for species A with a direction determined by the concentration gradient. The second driving force is along the growth direction due to bombardment-induced segregation, giving a mass flow of $J_A^{\rm BIS}$ for species A. Such a geometrically directional mass transfer mainly comes from two parts, the equilibrium segregation to reduce the free energy and radiation-induced segregation due to nonequilibrium defect flows. In the Au-Ni system under ion bombardment, both segregations are very strong. For an existing surface, ion bombardment of Au-Ni alloy at steady state produces a dynamical compositional profile normal to the surface in a subsurface zone [14]. The composition change may be described using a modified Cahn-Hilliard equation similar to the surface-directed spinodal decomposition [19], $\frac{\partial \phi}{\partial t} = M\nabla^2[-\phi + \phi^3 - \frac{1}{2}\nabla^2\phi + V(z)]$. But the surface potential $V(z)$ here should include not only equilibrium segregation but also radiation-induced segregation. We generally describe the self-organization process with these two driving forces. As film growth is initiated, bombardment-induced segregation results in an element (say A) depleted on the surface and enriched in the subsurface. At this time, the uphill diffusion flux $J_A^{\rm chem}$ has the same direction as $J_A^{\rm BIS}$ and enhances depletion of A on the surface. However, the newly advancing surface layer has a composition of A higher than the just buried surface layer since the surface composition before any diffusion is determined by deposition flux. As such, $J_A^{\rm chem}$ has the opposite direction at the near surface and the subsurface region. But the species redistribution is determined by the total diffusion flux $J_A^{\rm tot} = J_A^{\rm chem} + J_A^{\rm BIS}$. If $J_A^{\rm BIS}$ is dominant, the species A from newly deposited layer still serves as the source and is pumped into the subsurface region. As the active subsurface zone moves forward to the depleted region, the composition of A ultimately reaches a critical value below which $J_A^{\rm chem}$ towards the surface is dominant over $J_A^{\rm BIS}$ towards the subsurface. When this happens, the total flux reverses towards the surface and the composition of A at surface would be higher than the nominal one. Further addition of materials to the surface in the deposition would increase the composition of A of this buried layer since total fluxes at both sides are now towards this layer. Such a feedback loop [different from that in Ref. [7]] provides a pathway for self-organization of superlattices in deposition of phase-separated systems with strong bombardment-induced segregation. It is similar to surface-directed spinodal decomposition but in a dynamic fashion. Figure 3 gives a schematic of composition profile and competition of segregation and uphill diffusion fluxes in formation of compositional modulations.

To demonstrate this proposed mechanism, we performed kinetic Monte Carlo simulations using the ABV model for the description of an AB alloy with vacancies [20], in which we only considered the interplay of equilibrium segregation and phase separation in an advancing nanoscale subsurface diffusion zone for simplicity. Such consideration may correspond to a scenario for growth

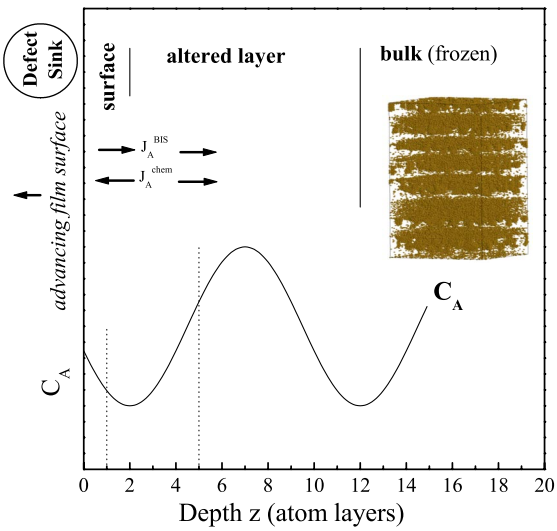

FIG. 3 (color online). Schematic illustration of concentration profile of species A (C_A) and mass flows at two different depths (dotted lines) in the nanoscale subsurface zone during the film growth. Two competing mass transports are uphill chemical diffusion ($J_A^{\rm chem}$) and bombardment-induced segregation flux ($J_A^{\rm BIS}$). Their interplay in the film growth can induce self-organization of compositional modulations along the growth direction. The inset shows a kinetic Monte Carlo configuration of $A_{0.075}B_{0.925}$ with the competing parameters $\beta J = -0.45$ and $\beta U = 0.3$.

of Au-Ni films under low-energy ion bombardment. Ion beams mainly enhance diffusion fluxes of equilibrium segregation and uphill diffusion in an ion penetrated subsurface zone. In the *ABV* model, the system Hamiltonian can be expressed as $H = H_0 + J\sum_{\langle i,j\rangle}\sigma_i\sigma_j + U\sum_{\langle i,j\rangle}(\sigma_i^2\sigma_j + \sigma_i\sigma_j^2) + K\sum_{\langle i,j\rangle}\sigma_i^2\sigma_j^2$, where spin variable σ_i $(1, -1, 0)$ represents that the site i is occupied by an A atom, B atom, or the vacancy, respectively. The parameter J determines the phase separation ($J < 0$) and the parameter U determines the segregation ($U \neq 0$). Specifically, the parameter U is related to the difference in surface energies of the two species. As shown in the inset of Fig. 3, strong competition of J and U (Au-Ni system has both strong phase separation and segregation) produces the compositional modulations along the growth direction in an asymmetric phase-separated alloy ($J < 0$ and $U \neq 0$) when the width of subsurface zone is large enough [21]. The *ABV* model we used is simple because we only considered the interplay of surface-energy induced segregation and phase separation. For a real system, such species redistribution may be kinetically assisted (or even dominated) by short circuit diffusion at grain boundaries and pinholes during film growth to reduce surface energy [22] as well as strain energy, particularly at low temperatures.

When the surface potential includes radiation-induced segregation (e.g., if we increased ion energy), the self-organization process becomes complicated. In the Au-Ni system, the equilibrium segregation flux for species Au is towards the surface [23]. However, the mass flow in radiation-induced segregation can be opposite to that in equilibrium segregation. In a typical IBAD the free surface serves as a major sink for defect annihilation [24]; the element that has a greater tendency to exchange with the vacancies would be depleted from the surface (inverse Kirkendall effect) if vacancy flux is dominant. In fact, for the Kirkendall effect in the Au-Ni system, it turns out that Au is the faster diffusing species at 900 °C, for the whole composition range of the Au-Ni solid solution [25]. This may also hold for the diffusion under ion bombardment [14]. Therefore, the net segregation flux in the Au-Ni system is determined by the competition of two opposite segregation fluxes and dependent on ion energy and flux. The wavelength of compositional modulations increases with ion energy because high energy ion bombardment would widen the altered layer and produce strong bombardment-induced segregation. Loss of this directional driving force may lead to a uniform spinodal decomposition as in the bulk even if it is on the nanoscale level. The ''kink'' for the Au-Ni system, where the superlattice structure varies nonlinearly with ion energy [see Fig. 2(b)], is mainly associated with competition from opposing segregation fluxes [26]. At intermediate ion energies, the mass flows of equilibrium segregation and radiation-induced segregation compete and cancel each other in such a degree that compositional modulations would be damped.

In summary, we demonstrated in the Au-Ni system that ion bombardment can produce superlattice structures in the film growth through the dynamic competition of mass transport along the growth direction. The interplay of bombardment-induced segregation and uphill diffusion is possibly responsible for the experimental observations. The periodicity of superlattices is on the order of few nanometers and they are tunable through changing ion energy and flux. We expect that this phenomenon can be observed in other similar systems.

J. H. He thanks the National Research Council for financial support.

*To whom correspondence should be addressed.
Email address: jhe@ccs.nrl.navy.mil

[1] A. Vailionis *et al.*, Phys. Rev. Lett. **85**, 3672 (2000).
[2] J. Nogami *et al.*, Phys. Rev. B **63**, 233305 (2001).
[3] P. M. Petroff *et al.*, Phys. Rev. Lett. **48**, 170 (1982).
[4] I. T. Ferguson *et al.*, Appl. Phys. Lett. **59**, 3324 (1991).
[5] S. P. Ahrenkiel *et al.*, Phys. Rev. Lett. **75**, 1586 (1995).
[6] P. Venezuela *et al.*, Nature (London) **397**, 678 (1999).
[7] Y. L. Foo *et al.*, Phys. Rev. Lett. **90**, 235502 (2003).
[8] I. Gerhards *et al.*, Phys. Rev. B **70**, 245418 (2004).
[9] T. B. Massalski, *Binary Alloy Phase Diagrams* (American Society for Metals, Metals Park, OH, 1986).
[10] J. H. He *et al.*, Phys. Rev. Lett. **86**, 2826 (2001); J. H. He *et al.*, Phys. Rev. Lett. **89**, 125507 (2002).
[11] R. E. Liesegang, Naturwiss. Wochenschr. **11**, 353 (1896); G. T. Dee, Phys. Rev. Lett. **57**, 275 (1986).
[12] R. A. L. Jones *et al.*, Phys. Rev. Lett. **66**, 1326 (1991).
[13] R. Kelly, Nucl. Instrum. Methods Phys. Res., Sect. B **39**, 43 (1989).
[14] N. Q. Lam, H. A. Hoff, and P. G. Régnier, J. Vac. Sci. Technol. A **3**, 2152 (1985); R. S. Li, J. H. Li, and T. Z. Hu, Appl. Surf. Sci. **68**, 123 (1993).
[15] S. B. Qadri, C. Kim, and M. Yousuf, Nucl. Instrum. Methods Phys. Res., Sect. B **190**, 817 (2002).
[16] H. G. Tompkins, J. Vac. Sci. Technol. **16**, 778 (1979).
[17] T. Bäck, *Evolutionary Algorithms in Theory and Practice* (Oxford University Press, New York, 1996); S. Yip and Y. H. Pao, IEEE Trans. Sys. Man Cybern. **24**, 1383 (1994).
[18] I. Daruka and J. Tersoff, Phys. Rev. Lett. **95**, 076102 (2005).
[19] S. Puri and K. Binder, Phys. Rev. E **66**, 061602 (2002).
[20] M. Porta, E. Vives, and T. Castán, Phys. Rev. B **60**, 3920 (1999).
[21] J. H. He *et al.* (to be published).
[22] G. L. Zhou, M. H. Yang, and C. P. Flynn, Phys. Rev. Lett. **77**, 4580 (1996).
[23] J. J. Burton, C. R. Helms, and R. S. Polizzotti, J. Vac. Sci. Technol. **13**, 204 (1976).
[24] M. V. RamanaMurty and H. A. Atwater, Phys. Rev. B **45**, R1507 (1992); J. Appl. Phys. **77**, 2351 (1995).
[25] M. J. H. van Dal *et al.*, J. Alloys Compd. **309**, 132 (2000).
[26] We observed with EDX that the composition of gold in the Au-Ni films is almost independent of ion energy and flux, ruling out preferential sputtering as well as uphill diffusion as a source of the kink effect in Fig. 2(b).